



ELSEVIER



International Journal of Hydrogen Energy III (III) III-III

International Journal of
**HYDROGEN
ENERGY**

www.elsevier.com/locate/ijhydene

Boron substituted carbon nanotubes—How appropriate are they for hydrogen storage?

M. Sankaran^a, B. Viswanathan^{a,*}, S. Srinivasa Murthy^b

^aNational Centre for Catalysis Research, Department of Chemistry, Indian Institute of Technology Madras, Chennai 600 036, India

^bMechanical Engineering Department, Indian Institute of Technology Madras, Chennai 600 036, India

Received 21 June 2007; accepted 9 July 2007

Abstract

The storage of hydrogen in carbon nanotubes requires appropriate chemical activators in suitable geometry. In this study, the role of boron substitution in carbon nanotubes is demonstrated for activation and storage of hydrogen.

© 2007 International Association for Hydrogen Energy. Published by Elsevier Ltd. All rights reserved.

Q1 Keywords: ■; ■; ■

1. Introduction

All three components of the hydrogen economy, namely, production, storage and application of hydrogen have been posing challenges to the scientific community for the past several decades. Developing a safe and reliable hydrogen storage technology that meets performance and cost requirements is critical to use hydrogen as a fuel for both vehicular and stationary power generation. Storage of hydrogen is attempted in various approaches involving gas phase storage with compressed hydrogen gas tanks, liquid hydrogen tanks and in solid substrates like metal hydrides, carbon-based materials/high surface area sorbants such as metal–organic frameworks (MOFs) and chemical hydrogen storage using complex hydrides. Among the various options of hydrogen storage, only storage in solid state materials seems to be promising. The scientific community in its anxiety and enthusiasm has come up with remarkable but not reproducible results for hydrogen storage in solid state. The desirable storage capacity for viable commercial exploitation of hydrogen as energy source is 6.5 wt% as postulated by US-DOE. However, any figure up to 67 wt% has been claimed as possible storage capacity in solids especially in carbon-based materials [1–4]. This situation is critical demanding definite and

exploratory solutions from practicing scientists. The essential questions that require immediate attention are:

- (i) Are the carbon materials appropriate for solid state hydrogen storage? 39
- (ii) If this is to be true, what types of materials or treatments for the existing carbon materials are suitable to achieve the desirable levels of hydrogen storage? 41
- (iii) What are the stumbling blocks in achieving the desirable storage of hydrogen in solid state? 43
- (iv) Where does the lacuna lie? Is it in the theoretical foundation of the postulate or is it in our inability to experimentally realize the desired levels of storage? 47

Against this background, the need for an activator for hydrogenation in carbon materials is realized, which should be easily hydridable than carbon and facilitate migration of the dissociated hydrogen to carbon surface. The pure carbon surface cannot activate hydrogen molecule, which is clear from the recent inelastic neutron scattering experiments which has shown that binding strength of hydrogen molecule is almost the same for all kinds of carbon materials and the magnitude of interaction is around 5 kJ/mol [5,6]. There must be strong interaction between the hydrogen and carbon surface (chemisorption) to give rise to high storage capacity. For chemisorption, the hydrogen molecule should be activated. When doping carbon

* Corresponding author.

E-mail address: bvnathan@iitm.ac.in (B. Viswanathan).

nanomaterials with alkali metal (Na, K), transition metals (Fe) and alloys (TiAl_{0.1}V_{0.04}, Ti–6Al–4V and NiO–MgO), the storage mechanism is different, as the metals involved form hydrides and the metal hydride could not store more than its number of atomic combinations [7–11]. The alternative may be heteroatoms like N, P, S and B. They seem to be promising as activators [12,13] by activating hydrogen molecule due to their hydriding property and the higher redox potential than carbon.

In this study the importance, gradation and the geometrical positions of boron substitution in carbon nanotubes (CNTs) for hydrogen activation were studied through density functional theory (DFT). In correlation to theoretical results, experiments were carried out to show the role of boron atoms for hydrogen activation. Pure CNTs and boron containing carbon nanotubes (BCNTs) were prepared by using various templates such as zeolite, clay and alumina membranes. The prepared pure and BCNTs have been characterized by XRD, Raman spectrum, IR, CP MAS NMR, TEM and high pressure hydrogen adsorption measurements. The variation of template and the carbon

precursor causes differences in the morphology. The chemical environment of boron and its relevance towards hydrogen storage application is also examined in correlation to theoretical results.

2. Computational methods

For the theoretical calculations the model has been constructed with three arm chair type (4,4) CNTs, which form a 3.65 Å inter tubular space as shown in Fig. 1. The details about the model construction and methodology used are given in our earlier communication [14]. The substitution of boron atoms are carried out at the edge positions of the nanotube, which show the minimum potential energy for the cluster. Computations using DFT have been carried out on the optimized configuration obtained using universal force field (UFF 1.02) parameter [15]. Cerius² software was used for the force field calculations and the single point energy calculations on the optimized configurations obtained from force field have been carried out using Gaussian 03 with Becke's three parameter hybrid function

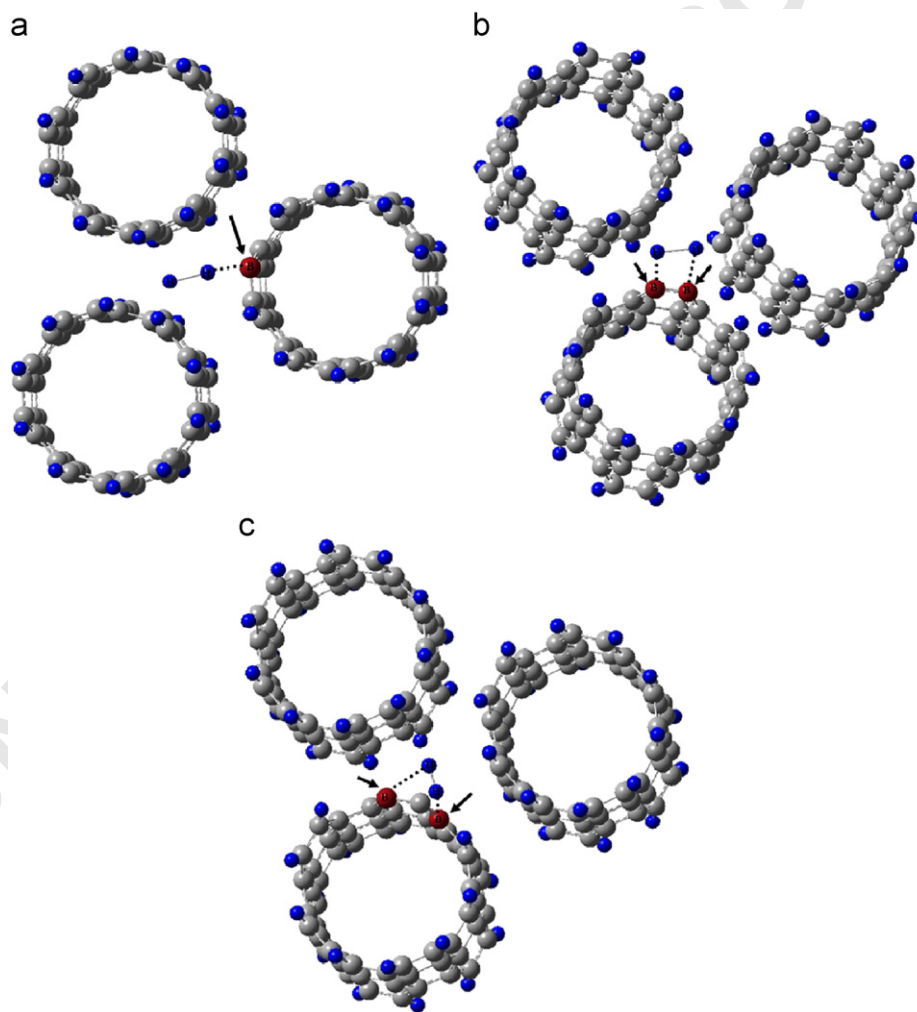


Fig. 1. (a) The hydrogen molecule interaction with the boron atom substituted in the UFF optimized CNT (4,4) cluster, where the terminal positions are saturated with hydrogen. (b) Hydrogen interaction with the boron atoms substituted in the adjacent positions of the carbon nanotube. (c) Hydrogen interaction with the alternate positions of the carbon nanotube (the arrow indicated are boron atom).

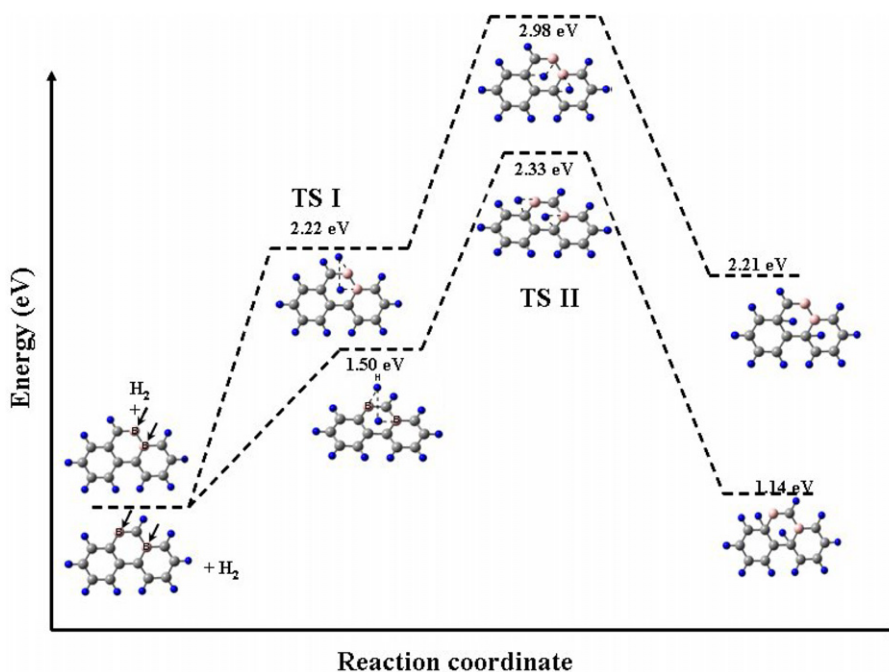


Fig. 2. The transition state energy profile of the boron substituted CNT cluster calculated by DFT method (B3LYP) with 6-31g (*p, d*) basis set.

with LYP correlation function (B3LYP) and 6-31G (*p, d*) as basis set [16–18]. The total energy, H–H bond distance as well as the dissociation energy of hydrogen was obtained from these calculations.

To study the reaction mechanism, a simple cluster model with 14 carbon atoms has been chosen. The cluster model is the terminal and reactive part in the SWNT for the hydrogen interaction and hydrogenation as shown in Fig. 2. The cluster was fully optimized with density functional B3LYP method with 6-31G (*p, d*) basis set. The nature of stationary points thus obtained was characterized by frequency calculations. All the transition states corresponding to hydrogen migration were located and characterized as saddle points using the frequency calculations. The geometric parameters and the nature of the imaginary frequencies were examined using the graphical interface program, Gauss View 03 [19]. All the DFT calculations were performed using Gaussian 03 in a cluster of IBM Linux machine.

3. Experimental section

3.1. Materials used

Tetrahydrofuran was dried over sodium and distilled before use. 1,4-Divinyl benzene and hydrofluoric acid, (all from Merck) were used as received. Acetylene (99.95%), hydrogen (99.98%) and argon (99.99%) were used with no further purification. Alumina template membranes (0.2 μm pore diameter and 60 μm thick) were obtained commercially (Whatman Anodisc Membrane Filters, Whatman Inc.). H-zeolite-Y (Sud Chmie Pvt Ltd., India) and Na-montmorillonite used for the preparation of Al-pillared clay. $\text{AlCl}_3 \cdot 6\text{H}_2\text{O}$ (S.D.

Fine-Chem Ltd., India) was used as source of aluminum ion for the preparation of Al-pillared clays. Helium (99.99%) and hydrogen (99.98%) were purified using a liquid nitrogen trap and activated carbon trap prior to hydrogen sorption experiments. Commercial activated carbons Calgon and CDX-975 were used to compare the hydrogen storage capacity with prepared CNTs.

3.2. Synthesis of pure and BCNTs

Pure carbon nanotubes (CNT1) were prepared by using polyphenylacetylene polymer as the carbon source by using alumina membrane as template. The polyphenyl acetylene/alumina composite was prepared by adding 10 ml of 5% w/w polyphenyl acetylene in dichloromethane to the alumina membrane applying vacuum from the bottom. The entire polymer solution penetrates inside the pores of the membrane by the mild suction applied. The solvent was evaporated slowly and the membrane was dried in vacuum at 373 K for 10 min. The composite was then polished with fine neutral alumina powder to remove the surface layers and ultrasonicated for 20 min to remove the residual alumina powder used for polishing. The composite was then carbonized by heating in argon atmosphere at 1173 K for 6 h at a heating rate of 10 K/min. This resulted in the deposition of carbon on the channel walls of the membrane. The carbon/alumina composite was then placed in 48% HF to free the nanotubes. The tubes were washed with distilled water to remove HF [20,21].

Boron containing carbon nanotubes (BCNT1) were prepared by using the boron containing polymer as the carbon precursor. Stable cross-linked π -conjugated hydroborane polymer prepared by hydroboration polymerization of 1,4-divinylbenzene

1 and diborane in THF medium. *In situ* polymerization has
2 been carried out over the alumina membrane template in THF
3 medium under nitrogen atmosphere. After the polymerization,
4 the membranes were removed and polished with alumina powder
5 to remove the adhered polymers. The polymer/alumina
6 composite membranes have been carbonized at 900 °C for
7 6 h in argon atmosphere. The carbon/alumina composite was
8 treated with 48% HF for 24 h to remove the template and
9 washed with distilled water followed by drying at 100 °C
10 (BCNT1).

11 Other pure and BCNTs were prepared by chemical vapour
12 deposition (CVD) method by using H-zeolite Y (CNT2 and
13 BCNT2) and Al-pillared clay (CNT3 and BCNT3) as template.
14 Al-pillaring of clay has been carried out using aluminum poly-
15 cationic species ($[Al_{13}O_4(OH)_{24}(H_2O)_{12}]^{7+}$) [22,23]. The
16 polycations are prepared by the partial base hydrolysis of a
17 dilute solution of aluminum chloride. Acetylene (5 ml/min) has
18 been used as a carbon source and for boron source *in situ* gen-
19 eration of borane gas by the addition of concentrated H_2SO_4 to
20 the $NaBH_4$ in THF medium, carbonized at 900 °C in argon at-
21 mosphere. The carbon/zeolite and carbon/clay composite have
22 been treated with 48% HF for 24 h and the undissolved carbon
23 was washed with distilled water and dried at 100 °C. Various
24 routes have been evolved for the synthesis of boron doped
25 nanotubes, including arc discharge, laser ablation, substitution
26 reactions and pyrolysis of precursors like acetylene–diborane
27 mixtures in a flow of helium and hydrogen [24–26]. In the arc
28 discharge and laser ablation techniques to produce CNTs, dif-
29 ficulties are encountered in the control of size and alignment
30 of the nanotubes. Further, these techniques require purification
31 processes to separate the CNTs from the catalyst particles used
32 in the synthesis. In the present case metal or metal oxide cat-
33 alyst were not used and this will avoid the presence of metal
34 impurities in CNTs and facilitates the study of the effect of
35 heteroatom alone.

3.3. Materials characterization

37 The BCNTs prepared were characterized by powder X-
38 ray diffraction using Shimadzu XD-D1 X-ray diffractometer
39 with Ni-filtered Cu K_α radiation ($\lambda = 1.5418 \text{ \AA}$). FT-IR Shi-
40 madzu 8400 series was used for IR studies in the range of
41 400–4000 cm^{-1} . Transmission electron micrographs (TEM)
42 were recorded with a JEOL-JEM 100SX microscope, working
43 at a 100 kV accelerating voltage. TEM sampling grids were
44 prepared by placing 2 μl of the sample dispersed in ethanol
45 solution on a carbon-coated grid and the solution was evap-
46 orated at room temperature. Scanning electron microscopic
47 (SEM) images were obtained using Philips XL 30 instru-
48 ment. Carbon and boron nuclear magnetic resonance (^{13}C -
49 and ^{11}B -NMR) have been utilized to investigate the chemical
50 environment of the CNTs. All MAS ^{13}C - and ^{11}B -NMR have
51 been recorded using BRUKER probe head with a zirconium
52 rotor of 4 mm diameter in Bruker AVANCE™ 400 MHz instru-
53 ment. Boric acid has been chosen as reference at 0 ppm for ^{11}B
54 NMR. The entire spectrum was recorded at a spinning speed
55 of 12 kHz.

3.4. Hydrogen absorption measurement

57 Volumetric low pressure and high pressure hydrogen adsorp-
58 tion measurements have been carried out using custom built
59 volumetric and Sievert's apparatus. The high pressure adsorp-
60 tion apparatus consists of reservoir cell and a cylindrical sam-
61 ple cell of known volume (33.8 cm^3). All possible care for the
62 possible sources of leak was carefully taken and long blank
63 run tests were carried out. Care has been taken to avoid the
64 errors due to factors such as temperature instability, leaks and
65 additional pressure and temperature effects caused by expand-
66 ing the hydrogen from the reservoir to the sample cell. The
67 volume of the system was determined by measuring accurately
68 those of the single components at lower pressures using heli-
69 um gas. The measurements were carried out by utilizing the
70 systematic procedure as follows: Typically the mass of the car-
71 bon samples used for hydrogen storage measurements is in the
72 region of 100–300 mg. Prior to measurement, the samples are
73 degassed and heated at 300 °C for approximately 6 h in vacuum
74 of 10^{-5} Torr. The whole system has been pressurized at the
75 desired value by hydrogen and change in pressure was moni-
76 tored. The change in the pressure was recorded by a pressure
77 transducer, after the equilibrium was reached. All the hydrogen
78 adsorption measurements have been carried out at room tem-
79 perature. The experiments have been repeated under the same
80 conditions for various pressures. The hydrogen compressibility
81 factors were utilized for the calculations.

4. Results and discussion

4.1. Theoretical study

83 The quantum chemical calculation has been carried on the
84 cluster model as shown in Fig. 1 to find the hydrogen in-
85 teraction in pure and boron substituted CNT. From the re-
86 sults, it appears that substitution of carbon by boron atom
87 appears to favour the activation and dissociation of hydro-
88 gen molecule. The total energy, H–H bond distance and the
89 dissociation energy of hydrogen molecule obtained from the
90 DFT calculation are given in Table 1. The essential out come
91 from the calculations are the dissociation energy of hydrogen
92 in its free state is 4.76 eV, and remains unaltered when it is
93 placed in between the pure CNTs (4.51 eV). The substitution
94 of boron atom in the CNT shows interesting results, such as
95 single boron substitution in CNT cannot activate the hydro-
96 gen molecule, whereas two boron atoms are essential for the
97 hydrogen activation. The dissociation energy of hydrogen for
98 single boron substitution is 5.95 eV whereas when two boron
99 atoms are substituted in adjacent positions the dissociation en-
100 ergy is reduced to 3.88 eV. It is further decreased to 0.28 eV
101 when two boron atoms are substituted in the alternate positions.
102 Though the calculated dissociation energy values are unreal-
103 istically small, they definitely indicate that the dissociation of
104 hydrogen molecule is a facile process on heteroatom substi-
105 tuted CNTs. Even though the calculated dissociation energy is
106 small, the process of hydrogen storage may involve other bar-
107 riers including mass transport and hence could not be achieved

Table 1

The bond length and dissociation energy of hydrogen on the CNTs calculated using B3LYP with 6-31g (*p, d*) basis set on the UFF optimized structure

Substitution	Total energy (Hartrees)	Bond length H ₁ – H ₂ (Å)	Dissociation energy (eV)
H ₂	–1.175	0.708	4.76
CNT	–3686.5502	–	–
CNT + H ₂	–3687.7161	0.776	4.51
BCNT	–3671.7254	–	–
BCNT + H ₂	–3672.9440	0.818	5.95
2BCNT (adjacent)	–3658.6666	–	–
2BCNT (adjacent) + H ₂	–3659.8092	0.913	3.88
2BCNT (alternate)	–3659.3491	–	–
2BCNT (alternate) + H ₂	–3660.3594	0.928	0.28

Table 2

The transition state optimized parameters of the cluster and the value of the activation energy calculated by B3LYP with 6-31G (*p, d*) basis set

Substitution	E^a I (eV)	E^a II (eV)	H ₁ –H ₂ (Å)	X–H (Å)	C–H ₁ ^b (Å)	C–H ₂ ^b (Å)
Two boron substituted CNT cluster (adjacent)	2.22	2.98	1.95	1.31	2.59	2.72
Two boron substituted CNT cluster (alternate)	1.5	2.33	2.95	1.47	1.47	2.34

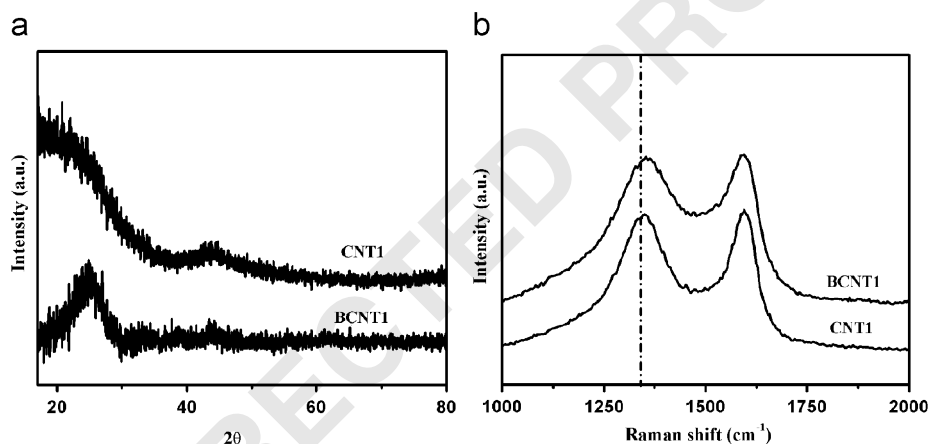
^a $E = E$ (transition state) – E (reactant).^bShortest C–H bond distance.

Fig. 3. X-ray diffraction pattern (a) and Raman spectra (b) of pure and boron containing carbon nanotubes (CNT1 and BCNT1).

1 at such low energies. From the calculation, it is observed that
 2 the substitution of boron at alternate positions is favourable
 3 for hydrogen activation rather than substitution at adjacent po-
 4 sitions. It can be substantiated that boron–boron bond length
 5 is a key factor for H–H bond activation. An alternate position
 6 of B substitution seems to be favourable for the activation of
 7 hydrogen, wherein bonding appears to be similar to that of
 8 diborane [27,28].

9 Essentially the hydrogen activation and subsequent hydro-
 10 genation of carbon atoms of BCNTs are conceived by the path-
 11 way shown in Fig. 2. In this alternate substitution configura-
 12 tion, the overall activation barrier is considerably reduced to
 13 nearly 1.5 eV, whereas for the situation of substitution at adja-
 14 cent positions the activation barrier is of the order of 2.22 eV.
 15 This is an indication that the substitution at alternate position
 16 is geometrically more favourable than adjacent substitution for
 17 hydrogenation of carbon atoms of CNT, while the C–H forma-

tion is not that favourable for the system where boron substi-
 18 tution is effected at adjacent position. The results substantiating
 19 these statements are given in Table 2.

4.2. Experimental study

4.2.1. Characterization of pure and BCNTs prepared by template assisted synthesis

4.2.1.1. CNTs prepared from alumina membrane as the tem-
 22 plate. X-ray diffraction study has been carried out on the
 23 CNTs produced by alumina membrane as template and the
 24 diffractograms are shown in Fig. 3a. The CNTs produced
 25 were graphitic in nature and the diffraction at $2\theta = 26^\circ$ cor-
 26 responds to (002) plane of hexagonal graphite (JCPDS car
 27 files, no. 41-1487). The graphitic natures of CNTs are mainly
 28 due to the carbonization of the carbon precursors at 900 °C.
 29 There exist a shift in the *d* value for (002) plane, which is
 30

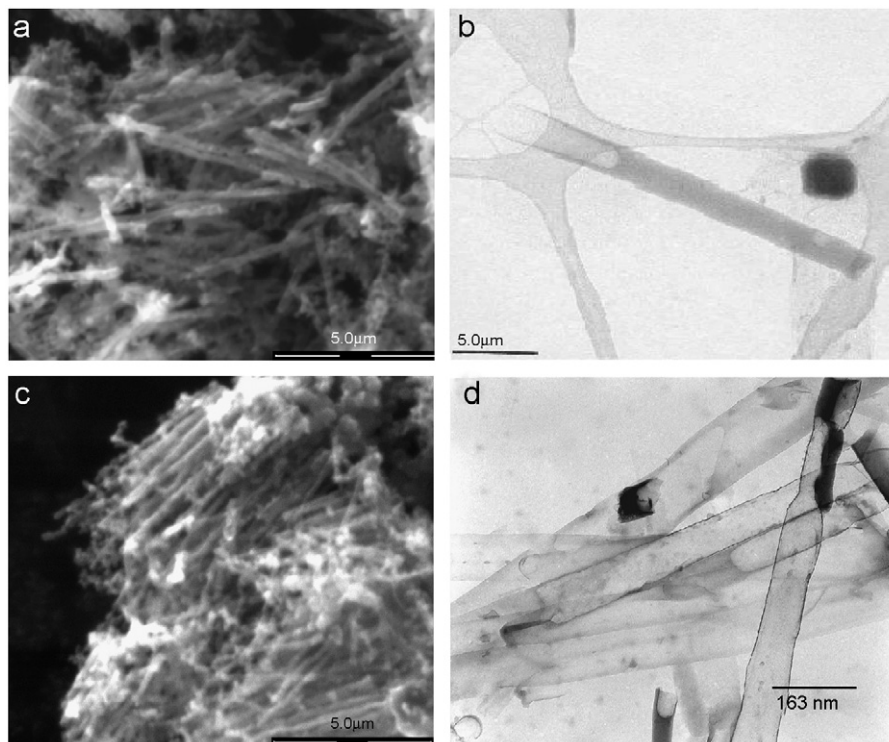


Fig. 4. (a and b) SEM and TEM images of the pure carbon nanotubes (CNT1), respectively, (c and d). SEM and TEM images of the boron substituted carbon nanotubes (BCNT1), respectively.

1 attributed to the substitution of boron in the carbon in the carbon network. The intensities of in-plane reflections particularly for the 110 reflection at $2\theta = 32^\circ$ are weaker in the case of BCNT1; this may be due to the presence of localized BC_3 domains slightly influencing the periodic atomic arrangement of the hexagonal carbon network [29].

7 Raman spectra (Fig. 3b) show the D-peak (1350 cm^{-1}) due to the disorder-induced phonon mode (breathing mode, A_{1g} -band) and the G-peak (1594 cm^{-1}) assigned to the Raman-allowed phonon mode (E_{2g} -band). The CNTs synthesized showed the same grade of disorderliness in the graphitic structure. The CNTs produced by the polymer precursor using alumina membrane as template show the same intensity of D and G band character. This is due to the more graphitic nature with higher degree of disorderliness. The disorder is created by the tubular morphology and the substitutional effect of boron in the CNTs. There also exists a shift in the Raman D-band due to the substitutional effect of boron in the carbon lattice.

19 From the SEM (Fig. 4a and c) the morphology of tubular and well-aligned bundles of pure and boron containing carbon nanotubes (CNT and BCNT1) samples are well seen.

23 The HR-TEM (Fig. 4b and d) of CNT1 and BCNT1 after the carbonization at 900°C for 6 h shows hollow tubes with slight deformation in the end of the tube, probably caused by the ultrasonication and vigorous HF treatment. Micrograph also indicates the formation of cylindrical, hollow and transparent tubes. The outer diameter of the tube is less than the (approximately 150 nm) channel diameter of the template used (also a layer of amorphous carbon on the wall of the tube is

seen). Though the carbon tubes produced by this method are not completely graphitic in nature, as those produced by arc-discharge process, their disordered structure is quite typical of fibres or nanotubes produced by decomposition of hydrocarbons, as is evident from the amorphous carbon on the wall of the CNT.

4.2.1.2. *CNTs prepared from zeolite as template.* The XRD pattern of CNTs prepared from zeolite as template is shown in Fig. 5a. The predominant (200) plane at $2\theta = 24.1^\circ$ of graphitic peak is observed for both CNT2 and BCNT2. However, BCNT2 showed a predominant peak at $2\theta = 32^\circ$ corresponds to (111) diffraction of boron carbide (boron carbide, JCPDS files, no. 86-1128). This recommends the presence of boron in carbon.

Raman studies (Fig. 5b) showed the graphitic D-band and G-band for the prepared CNTs using zeolite as template. The FWHM and the intensity of the D-band are higher than the G-band in BCNT2 compared to CNT2, which signify the greater disorderliness due to boron substitution in the CNTs. The D-band increases with increase in the disorder which is normally represented by the I_D/I_G ratio. Usually the I_D/I_G ratio increases with (i) increasing the amount of amorphous carbon in the material and (ii) decreasing the graphite crystal size. From the studies it is found that I_D/I_G ratio increased. This indicates the substitution of boron in the carbon frame work and decrease of the graphitization process.

The SEM images of CNT2 and BCNT2 showed amorphous and fibrous nature of the CNTs produced. Usually CNTs

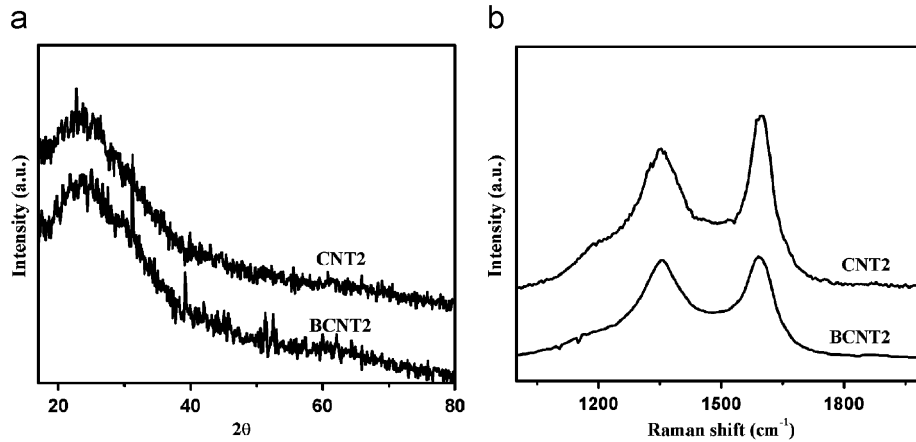


Fig. 5. (a and b) X-ray diffraction pattern and Raman spectra of pure and boron containing carbon nanotubes (CNT2 and BCNT2), respectively.

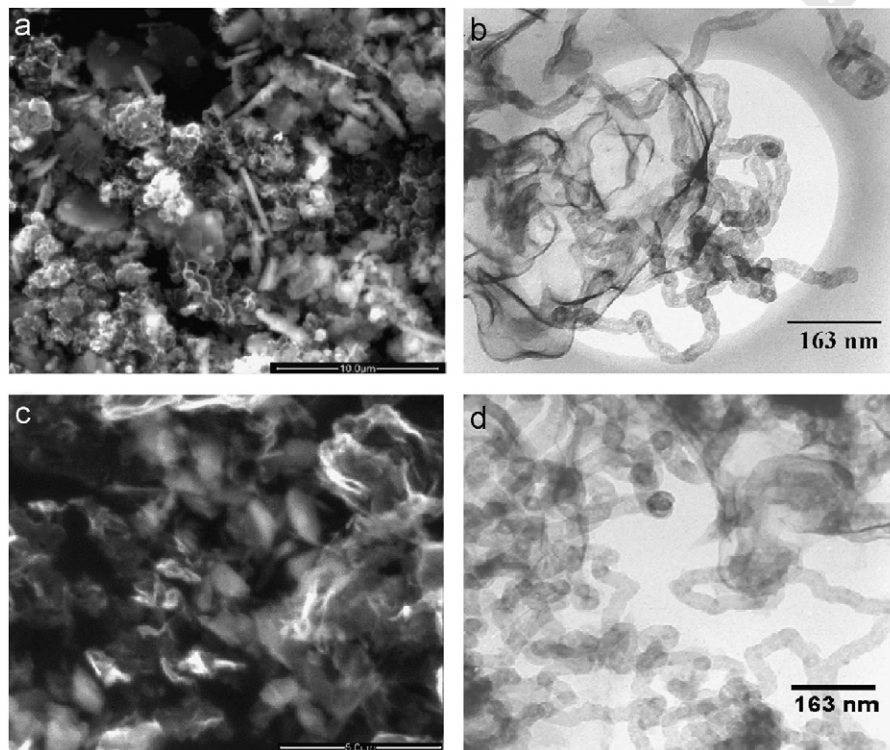


Fig. 6. SEM and TEM images of the carbon nanotubes: (a and c). SEM images of CNT2 and BCNT2 (b and d) TEM images of carbon nanotubes CNT2 and BCNT2 prepared from zeolite as template, respectively.

1 produced by CVD method leads to the formation of nanotubes with disordered structure, amorphous carbon and fibres
 3 [30,31], which as can be seen from the TEM images (Fig. 6b and d).

5 4.2.1.3. CNTs prepared from clay as template. The XRD pattern and Raman spectrum of CNT3 and BCNT3 are shown in
 7 Fig. 7. Graphitic nature of the CNTs produced is seen in Fig. 7a. Predominant (002) plane of graphite at $2\theta = 23.8^\circ$ and
 9 (001) plane at 2θ equal to 45.1° are viewed. BCNT3 showed a broad peak at $2\theta = 32^\circ$ corresponds to (111) diffraction of

boron carbide, indicates presence of boron in carbon lattice. From the Raman analysis, well-resolved D-bands and G-bands
 11 are shown for both the CNTs, where BCNT3 showed broad peaks with high FWHM compared to pure CNT3. This can be
 13 attributed to the increased disorderliness by boron substitution in the CNTs. The shift in the d -values is not significant by
 15 the substitution of heteroatom into the carbon lattice. However, Raman spectrum showed well-resolved D-band characteristic
 17 peak for destabilization. 19

SEM and TEM images of CNTs prepared from clay as template are shown in Fig. 8. SEM images showed layered type
 21

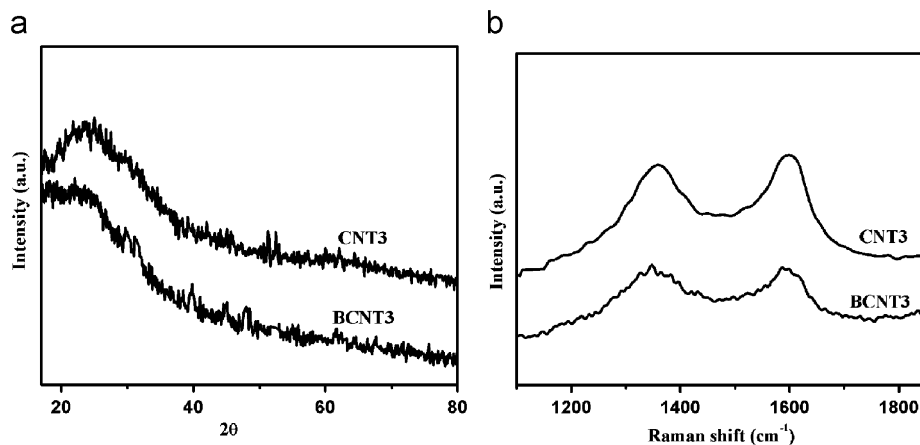


Fig. 7. (a and b) X-ray diffraction pattern and Raman spectra of pure and boron containing carbon nanotubes (CNT3 and BCNT3), respectively.

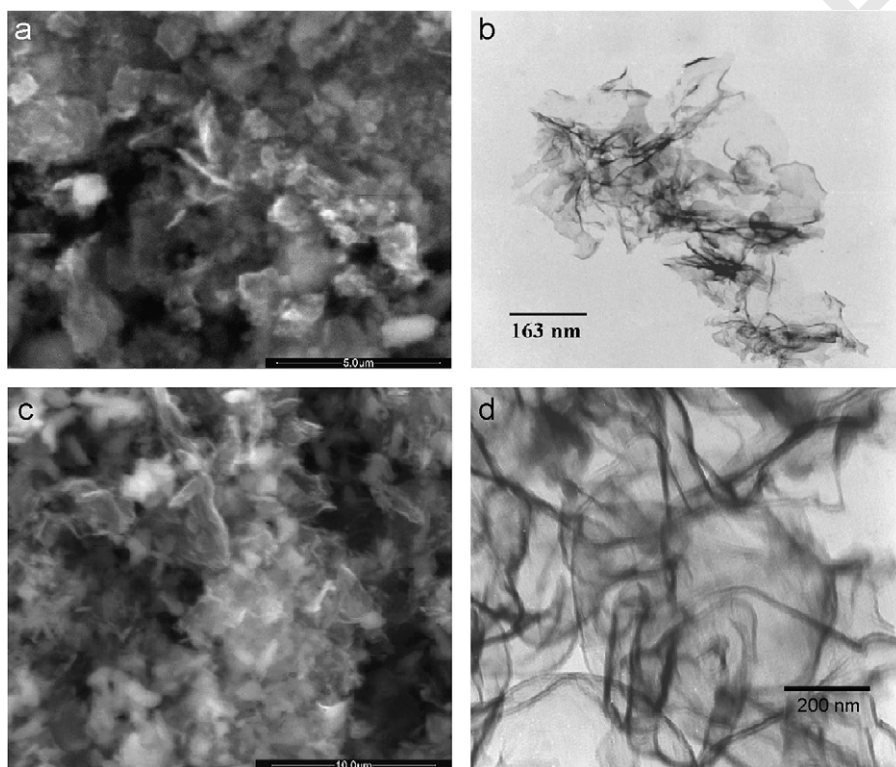


Fig. 8. (a and b) SEM and TEM pictures of pure carbon nanotube (CNT3) prepared from clay as template. (c and d) SEM and TEM images of boron containing carbon nanotubes (BCNT3), respectively.

1 structure with amorphous nature. Peculiarly BCNT3 showed
 3 layered structure with special open arrangement. TEM images
 5 showed layered and disordered structure with amorphous and
 7 fibrous carbon. Since no catalyst has been used for the synthesis
 of CNTs, it is worth pointing out that the nanotubes produced
 by template synthesis under normal experimental conditions
 are almost free from impurities.

9 **4.2.1.4. IR spectra of BCNTs.** The boron substitution in the
 carbon network displayed an effective downshift of the vibra-
 tions, which is attributed to the much lower force constant by

B–C than that of C–C force constant. The presence of band at
 1250 cm⁻¹ corresponds to C–B bond in all the samples (Fig.
 9). Usually C–B band occurs at 1050–1200 cm⁻¹ increase in
 the frequency is correlated to higher carbon contents [32]. This
 shows that the prepared CNTs are having higher carbon con-
 tents by the synthetic strategy applied. The formation of band at
 645 cm⁻¹ in the BCNTs (2 and 3) sample mainly corresponds
 to the B–B entity in the carbon network.

13
 15
 17
 19 **4.2.1.5. Solid state ¹³C & ¹¹B MAS NMR of BCNTs.** The
 chemical environment of the CNTs has been characterized

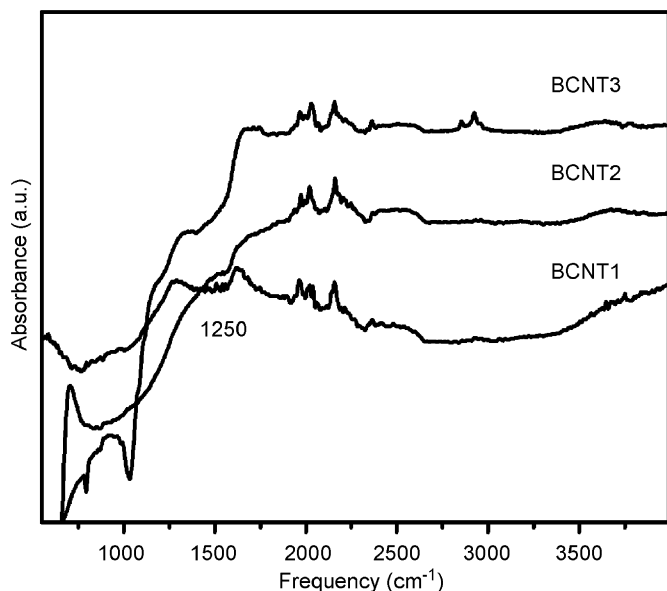


Fig. 9. FT-IR spectrum of the boron containing carbon nanotubes (BCNTs).

1 by NMR experiments. In the ^{13}C CP MAS NMR experiment
 2 graphitic nature of the CNTs are well evident from the spec-
 3 trum by the characteristic peak at 129 ppm (Fig. 10a) for the
 4 BCNT1. The ^{11}B MAS NMR experiment shows the environ-
 5 ment of boron in carbon network. In ^{11}B MAS NMR the dipolar
 6 interaction is only possible by the homonuclear B–B interac-
 7 tion, whereas in MAS condition the heteroatom ^{13}C shows very
 8 low nuclear spin and the interaction is negligible. Though the
 9 possibility of second-order quadrupole interaction is due to ^{11}B
 10 ($I = 3/2$), the MAS (magic angle spinning) does eliminate sec-
 11 ondary quadrupole interaction and the line shape is due to main
 12 interaction only. Second-order quadrupole interaction does not
 13 contribute to the line shape [29]. In the experiments two differ-
 14 ent chemical environments are observed for the BCNT1 which
 15 is prepared by polymer precursor route (Fig. 10b). There is a
 16 clear indication that boron atoms are bonded to carbon atom in
 17 two different environments and there is no possible quadrupole
 18 interaction due to B–B bond and also the hetero nuclear inter-
 19 action with ^{13}C is very weak. BCNT2 shows a broad spectrum
 20 and has the possibility of multiple environment and presence
 21 of B–B entity. These results reveal that boron atoms are present
 22 in two different chemical environments for BCNT1 prepared
 23 by polymer route.

4.2.2. Hydrogen absorption studies

25 Hydrogen absorption activity of CNTs have been carried
 26 out at various temperatures -196 , 25 , 100 and 150°C at
 27 0 – 760 mmHg pressure. The absorption at room temperature is
 28 negligible; however, absorption isotherm at 77 K shows that
 29 at this temperature the condensation of hydrogen is not possi-
 30 ble and it requires either low temperature of 20 K or higher
 31 pressure. The values of specific surface area (SSA) evaluated
 32 by BET method using nitrogen gas absorption at -196°C and
 33 the maximum hydrogen absorption at 760 mmHg of pressure
 for various temperatures are given in Table 3. From the re-

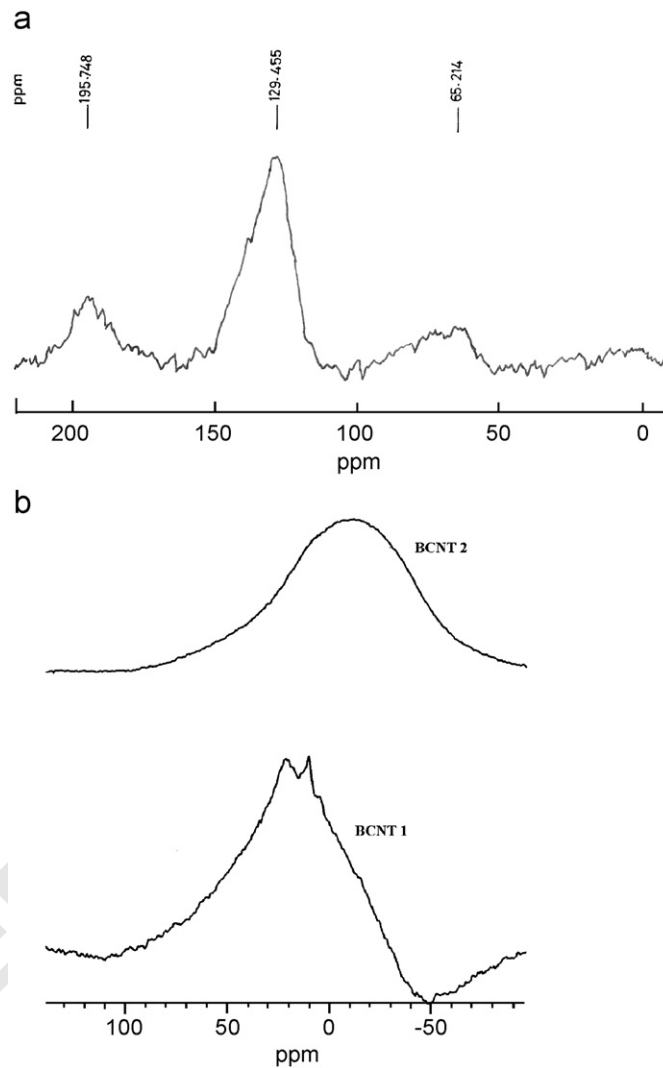


Fig. 10. (a) ^{13}C CP MAS NMR of BCNT1 and (b) ^{11}B MAS NMR spectrum of boron containing carbon nanotubes prepared by different methods (BCNT1 and BCNT2).

Table 3

The hydrogen absorption activity of carbon materials at different temperatures at 1 atm pressure and specific surface area measured by BET method

Samples	SSA (m^2/g)	Volume of hydrogen absorbed at 1 atm (cm^3/g) at various temperatures ($^\circ\text{C}$)			
		-196	25	100	150
BCNT1	523	127	–	16.5	–
CNT2	633	28.0	–	3.42	–
BCNT2	62.3	3.22	–	2.38	4.73
CNT3	48.8	–	–	3.0	–
BCNT3	32.7	1.09	–	1.7	–
CDX-975	325	28.1	0.53	2.83	4.18
Calgon	931	138	0.70	0.43	–

35 sults, it is seen that hydrogen absorption at -196°C showed
 36 a maximum of $1.2\text{ wt}\%$ for the boron containing carbon
 37 nanotubes (BCNT1) and high surface area Calgon activated
 carbon.

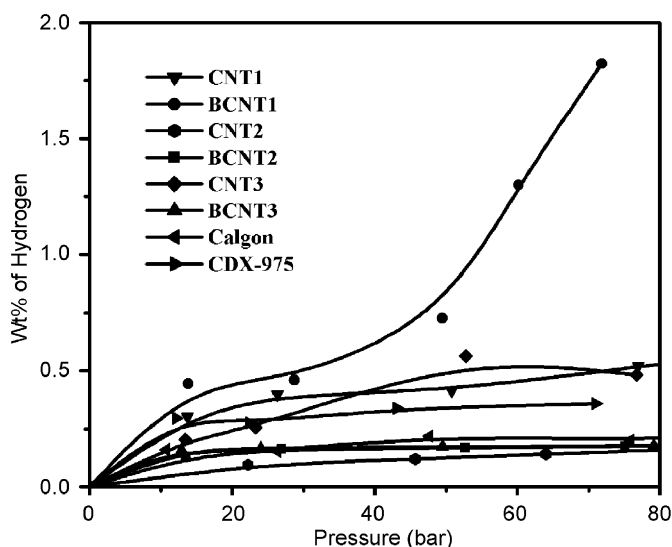


Fig. 11. High pressure hydrogen adsorption activity of various carbon materials.

High pressure hydrogen adsorption measurements (Fig. 11) show that the hydrogen storage capacity increases with pressure. A maximum storage capacity of 2 wt% at 80 bar pressure is obtained for BCNT1, whereas pure carbon nanotubes (CNT1) shows 0.6 wt%. Samples CNT2, BCNT2, CNT3 and BCNT3 show a maximum of 0.2 wt% at this pressure. The commercial samples also store hydrogen in the same order of magnitude with a maximum of 0.3 wt% for CX-975. These results show that there should be some activators needed to activate the hydrogen and boron substitution in carbon act as activators. These boron atoms should be incorporated suitably with appropriate geometrical and chemical environment for hydrogen activation. The results contented well with the theoretical predictions.

5. Summary

Theoretical studies have shown that the effective hydrogenation of CNTs is possible with activation centres and the BCNTs are able to activate the hydrogen in a facile manner compared to pure CNTs. For effective hydrogenation and hydrogen storage these boron atoms should be incorporated geometrically and chemically into the carbon network. BCNTs have been produced successfully by template assisted synthesis method. An effective and reproducible method of producing BCNTs with uniform pore diameter has been demonstrated by using alumina membrane as template. Use of different template and carbon sources results in variation of chemical environment of boron, which is identified by ^{11}B CP MAS NMR. BCNTs produced by using hydroborane polymer as the carbon precursor in alumina membrane template showed high hydrogen absorption activity. These materials show different chemical environments for boron with maximum < 2 wt% of hydrogen storage capacity at 80 bar and room temperature. This configuration has a bearing in hydrogen sorption characteristics.

Acknowledgements

We thank Council of Scientific and Industrial Research (CSIR), New Delhi, India, for the fellowship to one of us (M.S.) and MNRE Government of India, for financial support.

References

- [1] Dillon AC, Jones KM, Bekkedahl TA, Kiang CH, Bethune DS, Heben MJ. Storage of hydrogen in single-walled carbon nanotubes. *Nature* 1997;386:377–9. 37
- [2] Hynek S, Fuller W, Bentley J. Hydrogen storage by carbon sorption. *Int J Hydrogen Energy* 1997;22:601–10. 39
- [3] Chambers A, Parks C, Baker RTK, Rodriguez NM. Hydrogen storage in graphite nanofibers. *J Phys Chem B* 1998;102:4253–6. 41
- [4] Liu C, Fan YY, Liu M, Cong HT, Cheng HM, Dresselhaus MS. Hydrogen storage in single walled carbon nanotubes at room temperature. *Science* 1999;286:1127–9. 45
- [5] Schimmel HG, Kearley GJ, Nijkamp MG, Visser CT, de Jong KP, Mulder FM. Hydrogen adsorption in carbon nanostructures: comparison of nanotubes, fibres, and coals. *Chem Eur J* 2003;9:4764–70. 47
- [6] Ren Y, Price DL. Neutron scattering study of H_2 adsorption in single-walled carbon nanotubes. *Appl Phys Lett* 2001;79:3684–6. 49
- [7] Chen P, Wu X, Lin J, Tan KL. High H_2 uptake by alkali-doped carbon nanotubes under ambient pressure and moderate temperatures. *Science* 1999;285:91–3. 53
- [8] Pinkerton FE, Wicke BG, Olk CH, Tibbetts GG, Meisner GP, Meyer MS. et al. Thermogravimetric measurement of hydrogen absorption in alkali-modified carbon materials. *J Phys Chem B* 2000;104:9460–7. 55
- [9] Yang RT. Hydrogen storage by alkali-doped carbon nanotubes—revisited. *Carbon* 2000;38:623–6. 57
- [10] Hirscher M, Becher M, Haluska M, Quintel A, Skakalova V, Choi YM. et al. Hydrogen storage in carbon nanostructures. *J Alloys Comps* 2002;330:654–8. 61
- [11] Sankaran M, Viswanathan B. Hydriding of nitrogen containing carbon nanotubes. *Bull Catal Soc India* 2003;2:9–11. 63
- [12] Zhu ZH, Hatori H, Wang SB, Lu GQ. Insights into hydrogen atom adsorption on and the electrochemical properties of nitrogen substituted carbon materials. *J Phys Chem B* 2005;109:16744–9. 65
- [13] Sankaran M, Viswanathan B. The role of heteroatoms in carbon nanotubes for hydrogen storage. *Carbon* 2006;44:2816–21. 67
- [14] Rappe AK, Casewit CJ, Colwell KS, Goddard WA, Skiff WM. UFF, a full periodic table force field for molecular mechanics and molecular dynamics simulations. *J Am Chem Soc* 1992;114:10024–35. 71
- [15] Becke AD. Density-functional thermochemistry. III. The role of exact exchange. *J Chem Phys* 1993;98:5648–52. 73
- [16] Lee C, Yang W, Parr RG. Development of the Colle–Salvetti correlation-energy formula into a functional of the electron density. *Phys Rev B* 1988;37:785–9. 75
- [17] Frisch MJ, Trucks GW, Schlegel HB, Scuseria GE, Robb MA, Cheeseman JR. et al. Gaussian 03. Revision C.02. Gaussian Inc., Wallingford CT: 2004. 79
- [18] Dennington II R, Keith T, Millam J, Eppinnett K, Hovell WL, Gillil R. GaussView, Version 3.09. Semichem, Inc., K.S. Shawnee Mission; 2003. 81
- [19] Rajesh B, Thampi KR, Bonard JM, Xanthopoulos N, Mathieu HJ. et al. Carbon nanotubes generated from template carbonization of polyphenyl acetylene as the support for electrooxidation of methanol. *J Phys Chem B* 2003;107:2701–8. 83
- [20] Rajesh B, Karthikeyan S, Bonard JM, Thampi KR, Viswanathan B. Carbon nanotubes generated from polyphenyl acetylene. *Eurasian Chem Tech J* 2001;3:11–6. 87
- [21] Vaccari A. Preparation and catalytic properties of cationic and anionic clays. *Catal Today* 1998;41:53–71. 89
- [22] Figueras F. Pillared clays as catalysts. *Catal Rev Sci Eng* 1988;30:457–99. 91
- [23] Borowiak-Palen E, Pichler T, Fuentes GG, Graff A, Kalenczuk RJ, Knupfer M. et al. Efficient production of B-substituted single-wall carbon nanotubes. *Chem Phys Lett* 2003;378:516–20. 95

- 1 [24] Han W, Bando Y, Kurashima K, Satom T. Boron-doped carbon nanotubes
3 prepared through a substitution reaction. *Chem Phys Lett* 1999;299:368
5 –73.
- 7 [25] Golberg D, Bando Y, Han W, Kurashima K, Sato T. Single-walled B-
9 doped carbon, B/N-doped carbon and BN nanotubes synthesized from
11 single-walled carbon nanotubes through a substitution reaction. *Chem
Phys Lett* 1999;308:337–42.
- [26] Sankaran M, Muthukumar K, Viswanathan B. Boron substituted
fullerene—can they be one of the options for hydrogen storage?.
Fullerene Nanotubes Carbon Nanostr 2005;13:43–52.
- [27] Weast RC. *Handbook of chemistry and physics*. 59th ed., Boca Raton:
CRC Press; 1978 p. F217.
- [28] Shirasaki T, Derré A, Ménétrier M, Tressaud A, Flandrois S. Synthesis
and characterization of boron-substituted carbons. *Carbon* 2000;38:1461
–7.
- [29] Colomer JF, Bister G, Willems I, Konya Z, Fonseca A, Van Tendeloo
G. et al. Synthesis of single-walled carbon nanotubes by catalytic
decomposition of hydrocarbons. *Chem Commun* 1999;10:1343–4.
- [30] Ci L, Xie S, Tang D, Yan X, Li Y, Liu Z. et al. Controllable growth
of single wall carbon nanotubes by pyrolyzing acetylene on the floating
iron catalysts. *Chem Phys Lett* 2001;349:191–5.
- [31] Shirai K, Emura S, Gonda S, Kumashiro YY. Infrared study of amorphous
 $B_{1-x}C_x$ films. *J Appl Phys* 1995;78:3392–400.

UNCORRECTED PROOF